Integrative Biology

Dynamic Article Links

Cite this: *Integr. Biol.*, 2012, **4**, 531–539

www.rsc.org/ibiology

PAPER

Surface mobility regulates skeletal stem cell differentiation

Cristina González-García,[a] David Moratal,[a] Richard O. C. Oreffo,[b] Matthew J. Dalby*[c] and Manuel Salmerón-Sánchez*[ad]

Received 14th October 2011, Accepted 11th February 2012
DOI: 10.1039/c2ib00139j

A family of polymer substrates which consists of a vinyl backbone chain with the side groups $–COO(CH_2)_xH$, with $x = 1, 2, 4$, was prepared. Substrates with similar chemical groups but decreasing stiffness, characterized by their elastic modulus at 37 °C, as well as surface mobility, characterized by the glass transition temperature, were obtained. We have investigated whether these subtle variations in polymer chemistry lead to alterations in fibronectin (FN) adsorption and mesenchymal stem cell response. The same FN density was adsorbed on every substrate ($\sim$450 ng cm^{-2}) although the supramolecular organization of the protein at the material interface, as obtained with AFM, was different for $x = 1$ and the other two surfaces ($x = 2, 4$). Consequently, this allows one to investigate the effect of physical properties of the matrix on stem cell differentiation after ruling out any influence of protein activity. Cell adhesion was quantified by calculating the size distribution of focal adhesions. Mesenchymal stem cell differentiation to the osteoblastic lineage was determined by quantifying protein levels for osteocalcin, osteopontin and Runx2, in the absence of any additional osteogenic soluble factors in the culture media, but as a direct effect of material properties. The findings indicate the potential to modulate skeletal progenitor cell commitment to the osteoblastic lineage through surface mobility of the underlying material surface.

Introduction

Mesenchymal or skeletal stem cells are able to differentiate along the stromal lineage to give rise to osteoblasts, chondrocytes and adipocytes through the application, typically, of chemical cues and specific factors.[1,2] There is also a wealth of emergent data that mesenchymal or skeletal stem cells are highly sensitive to their environment and, when cultured on synthetic substrates, these cells respond to cues provided by chemistry, stiffness, surface topography and dimensionality (2D *vs.* 3D), which are able to direct skeletal stem cell lineage differentiation.[3–10]

Cell–material interactions occur through a layer of matrix proteins including fibronectin (FN), vitronectin, fibrinogen and laminin that interface living cells and synthetic surfaces.[11–15] The concentration, distribution, and motility of the adsorbed protein layer on a surface play a fundamental role in the biofunctionality of a synthetic material. Thus it may be possible to manipulate these parameters to augment the biological

[a] *Center for Biomaterials and Tissue Engineering, Universitat Politècnica de València, 46022 Valencia, Spain. E-mail: masalsan@fis.upv.es; Fax: +34 963877276; Tel: +34 963877275*
[b] *Bone and Joint Research Group, University of Southampton Medical School, Southampton, UK*
[c] *Center for Cell Engineering, Institute of Biomedical and Life Sciences, University of Glasgow, Glasgow, UK. E-mail: m.dalby@bio.gla.ac.uk; Tel: +44 (0)141 330 3550*
[d] *CIBER de Bioingeniería, Biomateriales y Nanomedicina (CIBER-BBN), Valencia, Spain*

Insight, innovation, integration

This work identifies surface mobility as a novel mechanism able to regulate the differentiation of skeletal stem cells. Moreover, it points out the importance of investigating the intermediate layer of proteins at the cell–material interface before discussing the effect of any physical properties of the matrix (*e.g.* stiffness) on cell differentiation. To do that, we have synthesized a family of polymers with subtle variations in chemistry and qualitatively different stiffness and surface mobility, which lead to alterations in fibronectin (FN) adsorption and human mesenchymal stem cell behavior. Our findings identify surface mobility as a key factor able to regulate skeletal stem cell differentiation with wider implications therein for the modulation and manipulation of stem, progenitor and adult populations in hard and soft tissue regeneration. This paper integrates technology and biology in two ways: the preparation of material surfaces able to direct cell differentiation making use of a novel surface property (mobility), as well as the methodology developed to quantify cell differentiation through image analysis of secreted proteins.

response of a cell to a substrate.[16] Cell–substrate (protein) interactions are primarily *via* integrins, a family of transmembrane cell adhesion receptors.[17] Integrin-mediated adhesion is a complex process that involves integrin association with the actin cytoskeleton and clustering into focal adhesions: supramolecular complexes that contain structural proteins (such as vinculin, talin, tensin) and signaling molecules (focal adhesion kinase (FAK), *etc.*).[17,18] Thus, the initial cell–material interaction is a complex multi-step process whereby early events, such as adsorption of proteins, followed by cell adhesion and spreading, determine late biological events, typically, those related to cell growth, differentiation, matrix deposition and cell function.

It is recognised that the mechanical properties of the matrix are known to influence cell behavior regardless of the protein coating of the substrate. Differentiated cells such as fibroblasts, muscular VSMC cells, chondrocytes and neurons, cultured on rigid/stiff substrates, have been shown to develop micron-sized focal adhesions connected by actin fibers. However, these focal adhesion structures are gradually lost as cells are grown on softer matrices, as obtained by, for example, changing the crosslinking density of gels.[19–22] There is evidence from Ryan and colleagues that cell spreading and motility are enhanced on stiff substrates in comparison to soft surfaces (which favors cell–cell interaction and leads to more dense cell aggregates).[23] Furthermore, cell proliferation has been shown to be increased on stiff surfaces and, in the case of a rigidity gradient on the substrate, cells migrate to stiffer regions (durotaxis).[24–26]

Seminal work from Engler *et al.* provided the first evidence that matrix elasticity can direct stem cell lineage specification in the absence of soluble induction factors.[4] The authors showed that stem cells expressed markers for neurogenic, myogenic or osteogenic lineages when cultured on substrates mimicking neural, muscle and bone stiffness respectively.[3,4,27–29] However, the preparation of substrates with controlled rigidity often leads to small variations in substrate chemistry, as observed in changing the crosslinking ratio in a polyacrylamide gel.[4,20] In addition some studies suggest that these changes in themselves lead to subtle variations in surface chemistry and alter protein adsorption that as a consequence alters cell behavior.[30,31]

The current work has investigated mesenchymal stem cell differentiation on a family of FN-coated polymers whose physical properties (stiffness and surface mobility) could be modulated by discrete variations in material chemistry—for example the sequential addition of methyl groups in the side group of a vinyl chain. FN was adsorbed on the different substrates and its supramolecular organization characterised by AFM. FN adsorption, in terms of the surface density and conformation, was noted to not occur equally on each test substrate. Subtle variations in surface chemistry were noted and these led to a non-monotonical dependence of mesenchymal stem cell differentiation in response to the physical properties of the matrix. Our findings identify surface mobility as a key factor able to regulate skeletal stem cell differentiation with wider implications therein for the modulation and manipulation of stem, progenitor and adult populations in hard and soft tissue regeneration.

Materials and methods

Materials

Polymer sheets were obtained by radical polymerization of a solution of the corresponding alkyl acrylate, *i.e.* methyl (MA), ethyl (EA) and butyl (BA) (Sigma-Aldrich, Steinheim, Germany), using 0.2 wt% benzoin (98% pure, Scharlau, Barcelona, Spain) as a photoinitiator. The polymerization was carried out up to limiting conversion. After polymerization, low molecular-mass substances were extracted from the material by drying *in vacuo* to constant weight. Thin films were prepared by making use of a spin-coater (Brewer Science, Rolla, USA). To do that, each one of the synthesized polymers was dissolved in toluene at a concentration of 2 wt%. Spin casting was performed on 12 mm glass coverslips at 2000 rpm for 30 s. Samples were dried *in vacuo* at 60 °C before further characterisation. The obtained films are not porous and approximately 500 nm in thickness.

Water contact angles were measured using a Dataphysics OCA. The volume of the drop was 20 μL and the measurement was performed after 10 s of substrate–water contact.

Mechanical measurements were performed using a Perkin Elmer DMA device in the traction mode. The elastic modulus was recorded as a function of temperature; from −50 °C to 50 °C. Specimens were bars *ca.* 5 × 8 × 1 mm.

Atomic force microscopy, AFM

AFM experiments were performed using a Multimode AFM equipped with a NanoScope IIIa controller from Veeco (Manchester, UK) operating in tapping mode in air; the Nanoscope 5.30r2 software version was used. Si-cantilevers from Veeco (Manchester, UK) were used with a force constant of 2.8 N m^{-1} and a resonance frequency of 75 kHz. The phase signal was set to zero at a frequency 5–10% lower than the resonance one. The drive amplitude was 600 mV and the amplitude setpoint Asp was 1.8 V. The ratio between the amplitude setpoint and the free amplitude Asp/A_0 was kept equal to 0.8.

Protein adsorption

Fibronectin from human plasma (Sigma, Barcelona, Spain) was adsorbed on the different substrates by immersing the material sheets in a solution of concentration 20 μg mL^{-1} in PBS for 10 min. After adsorption, samples were rinsed in PBS to eliminate the non-adsorbed protein. Remaining drops on the surface were removed by exposing the sample to a nitrogen flow for 2–3 minutes. AFM was performed in the tapping mode immediately after sample preparation. Height, phase and amplitude magnitudes were recorded simultaneously for each image.

To quantify the amount of adsorbed fibronectin, we measured the remaining protein in the supernatant, *i.e.* the amount of protein that remained in solution without adsorbing on the material surface, as explained elsewhere.[32] Different aliquots of non-adsorbed protein on substrates were subjected to 5%-SDS polyacrylamide gel electrophoresis (PAGE), using Laemmli buffer 2× and denaturing standard conditions. Proteins were transferred to a positively charged polyvinylidene difluoride nylon membrane (GE Healthcare) using a semidry transfer cell system (Biorad), and blocked by immersion in 5% skimmed milk in PBS for 1 h at room temperature. The blot was incubated with anti-human

fibronectin polyclonal antibody (developed in rabbit, Sigma) (1 : 500) in PBS containing 0.1% Tween-20 and 2% skimmed milk for 1 h at room temperature and washed three times (10 min each) with PBS containing 0.1% Tween-20 and 2% skimmed milk. The blot was subsequently incubated in horseradish peroxidase-conjugated donkey anti-rabbit immunoglobulin G (GE Healthcare) diluted 1 : 20 000 PBS containing 0.1% Tween-20 and 2% milk (1 h at room temperature). The enhanced chemiluminescence detection system (GE Healthcare) was used according to the manufacturer's instructions prior to exposing the blot to an X-ray film for 1 min.

Image analysis of the western bands was done using in house software developed under MATLAB R2009b (The MathWorks, Inc., Natick, MA, USA). All the western blotting bands were digitized using the same scanner (Epson Stylus Photo RX500, Seiko Epson Corp., Nagano, Japan) and the same scan parameters: 8 bits gray scale image and 300 dpi. The digitized images were binarized using Otsu's method, which chooses the threshold that minimizes the intraclass variance of the thresholded black and white pixels, in order to create a mask that automatically selected the edge of each western blot band.[33] This mask was applied to a negative version of the original scanned picture providing a resulting image that contained only the western bands. The last step of the process consisted finally in adding all the pixels that conformed each band correctly weighted by its intensity level.

Cell culture

Human bone marrow stromal cells were obtained from hematologically normal patients undergoing routine hip-replacement surgery as described previously with full ethical approval and patient consent.[34] Skeletal/mesenchymal stem cell populations were enriched from the bone marrow stromal cell population with Stro-1 selection using magnetic activated cells sorting (MACS) as previously detailed.[35] Stro-1 has been used as a stringent marker for enhancing the most primitive multipotent population of the bone marrow.[36–39] Thus, these cells can be used at very low passage preventing phenotypical drift due to prolonged culture/excessive passaging. Prior to seeding on FN-coated substrates, STRO-1+ cells were cultured in 75 cm^2 tissue culture flasks and cells were maintained in basal medium (αMEM supplemented with 10% foetal bovine serum and 2% antibiotics) at 37 °C. All cells used in this study were from passage 3 or lower.

Sample disks (12 mm diameter) previously sterilized in UV for 1 h and placed in a 24-well tissue culture plate were hydrated with PBS and coated with FN 20 μg mL^{-1} (1 h at room temperature). Then, 1×10^4 cells were placed onto each substrate and the experiments were carried out in αMEM medium under serum-free conditions at 37 °C in a humidified atmosphere under 5% CO_2 for 2 h, in order to study the initial adhesion on FN coated substrates. After that, the medium was changed to αMEM medium with 10% FBS, in order to provide the necessary nutrients during the incubation time, and the substrates were incubated at 37 °C for different times: 3 days for cell adhesion, 1 day to detect the phosphorylation of Runx2, and 21 days for osteocalcin (OCN) and osteopontin (OPN) expression. The medium was replaced after one culture day in all experiments, and it was changed twice weekly in experiments of 21 days. Each experiment was performed in triplicate.

Immunofluorescence (vinculin, Runx2, OPN, OCN)

After different culture times, MSCs were washed in phosphate buffered saline (PBS) and fixed with 4% formaldehyde (Fisher) with 2% sucrose in phosphate-buffered saline (PBS), at 37 °C for 15 minutes. Afterwards, the samples were rinsed with PBS and a permeabilising buffer (10.3 g sucrose, 0.292 g NaCl, 0.06 g $MgCl_2$, 0.476 g Hepes buffer, 0.5 mL Triton X, in 100 mL PBS, pH 7.2) was added at 4 °C for 5 minutes. The samples were saturated then with 1% BSA/DPBS at 37 °C for 5 minutes. Subsequently they were incubated at 37 °C for 1 h with primary antibody against vinculin (monoclonal mouse antibody, Sigma, 1 : 150) and with rhodamine-conjugated phalloidin (Invitrogen, 1 : 50) to stain actin; or phosphoRunx2 (rabbit polyclonal, Abgent, 1 : 100), or OPN (mouse monoclonal, Autogen Bioclear, 1 : 50), or OCN (mouse monoclonal, Autogen Bioclear, 1 : 50), all of them dissolved in 1% BSA in PBS. After three washes with PBS/0.5% Tween 20, the appropriate biotinylated anti-mouse or anti-rabbit secondary antibody (Vector Laboratories, 1 : 50) was incubated for 60 minutes at 37 °C, followed by fluorescein streptavidin tertiary label (Vector Laboratories, 1 : 50) for 30 minutes at 4 °C. Finally the samples were rinsed in PBS three times before mounted in Vectashield containing DAPI staining (Vector Laboratories). Secondary and tertiary antibody controls were performed for these cells. An Axiovert 200 M fluorescence microscope was used for imaging.

Image analysis

All image processing and analysis were done using an in house software developed under MATLAB R2009b (The MathWorks, Inc., Natick, MA, USA).

The size distribution of the focal plaques was determined through a several-step image analysis including a contour delineation of the cell. For a perfect segmentation of the cell, (i) images showing the actin cytoskeleton were grayscaled and equalized. (ii) The cell was then detected (segmented); since the cytoskeleton differed greatly in contrast from the background image, a gradient-magnitude method (Sobel)[40–42] was applied to the image and once the gradient image was calculated, a binary mask was created containing the segmented cytoskeleton. (iii) Compared to the original image, the binary gradient mask showed gaps in the lines surrounding the cell (the outline of the object of interest was not completely delineated). These linear gaps disappeared when the Sobel image was dilated using linear structuring elements (a vertical structuring element followed by a horizontal one), obtaining a clear and perfect contour detection of the cell. Once the cell was correctly segmented, the obtained binary mask was then applied to the image obtained in the red channel for vinculin. This permitted focus on the cell and the focal adhesions, as any other object in the image was virtually erased. This new image was then binarized through Otsu's method and size-filtered to avoid any extra small particles in the image that did not represent focal plaques whose sizes need to be determined.[33] Once the sizes of the focal contacts were determined, a size distribution was easily obtained.

To quantify the level of differentiation markers from fluorescence images (osteocalcin, osteopontin, phosphoRunx2), images were firstly equalized, providing an output grayscale image with its intensity values evenly distributed throughout the intensity range. Afterwards, they were segmented into 5 different classes by means of Otsu's multiple thresholding method.[33] Each class was then size-filtered using an opening morphological operator to eliminate remaining isolated pixels and the existing gaps were filled using an erosion morphological operator followed by a dilation one, using a diamond structuring element of size 3. The calculus of the intensity and the area covered by the 3 most brightest classes of the 5 different ones into which the image was segmented previously was then easily performed.

Statistics

All experiments were performed at least three times, in triplicate, unless otherwise noted. Data are reported as mean ± standard error. Results were analyzed by one-way ANOVA using SYSTAT 8.0 (SPSS). If treatment level differences were determined to be significant, pair-wise comparisons were performed using a Tukey post hoc test. A 95% confidence level was considered to be significant.

Results

Material properties

The material substrates in this study consist of a vinyl backbone chain with the side groups $-COO(CH_2)_xH$, with $x = 1, 2, 4$ (Fig. 1a). Surface wettability for these substrates remained approximately constant at 80° (Fig. 1b). In contrast, the elastic moduli (matrix elasticity) were observed to decrease monotonically as the number of methyl groups in the side chain increased, without modifying any other functionality of the system (Fig. 1c). Similarly, the glass transition temperature of the system, a dynamic property that accounts for the mobility of the polymer chains, decreased from 10 °C to −50 °C as x moved from 1 to 4. Topography of the surfaces was examined by AFM prior to protein adsorption. Similar roughness parameters were obtained regardless of the polymer composition (R_a = 20 nm and R_{ms} = 25 nm). In addition, we scanned the surface of the materials following immersion in PBS (in the absence of FN) and no significant modification in roughness was found. This family of materials provides a system with minimal variations in surface chemistry, similar wettability and qualitatively different stiffness and surface mobility.

Fibronectin adsorption

The surface density of adsorbed FN was quantified by western blot to analyse the amount of protein present in the supernatant following adsorption on the material surface. A calibration curve was built by loading gels with known amounts of FN and the resulting bands quantified by image analysis making use of Otsu's algorithm to systematically identify the band borders.[33] Each experiment of FN adsorption included the loading in the gel of two known amounts of FN (reference points) that correspond to points included in the calibration curve (allowing the position of the whole calibration curve to be verified for each adsorption experiment).[32] Fig. 2a shows

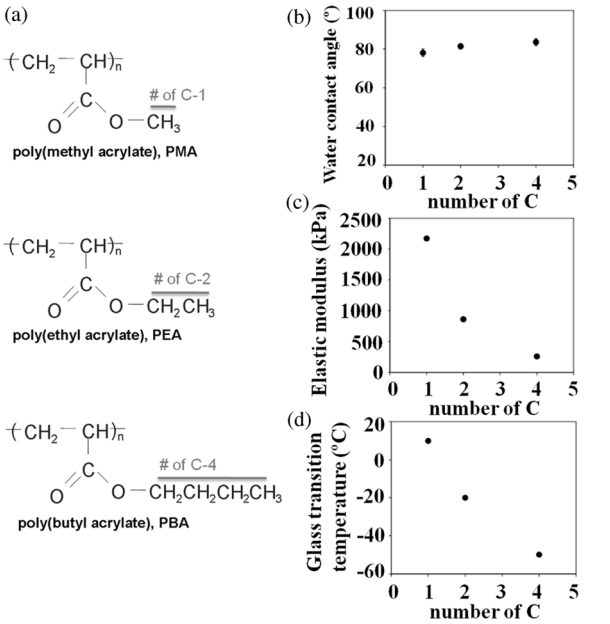

Fig. 1 Properties of the material substrates. (a) Chemical structure of the different substrates with increasing length of the side group: methyl (PMA), ethyl (PEA) and butyl (PBA). (b) Water contact angles of the different substrates as a function of the length of the side group (number of C). (c) Substrate's elastic modulus as a function of the length of the side group (number of C) as obtained at 37 °C. (d) Glass transition temperature of different substrates as a function of the length of the side group (number of C). The standard deviation of five independent measurements is included. Where not visible, it is lower than the size of the symbol.

the surface density of FN on the different materials after adsorption from a solution of concentration 20 μg mL^{-1}. The amount of adsorbed protein remains approximately constant (450 ng cm^{-2}) among surfaces (Fig. 2a).

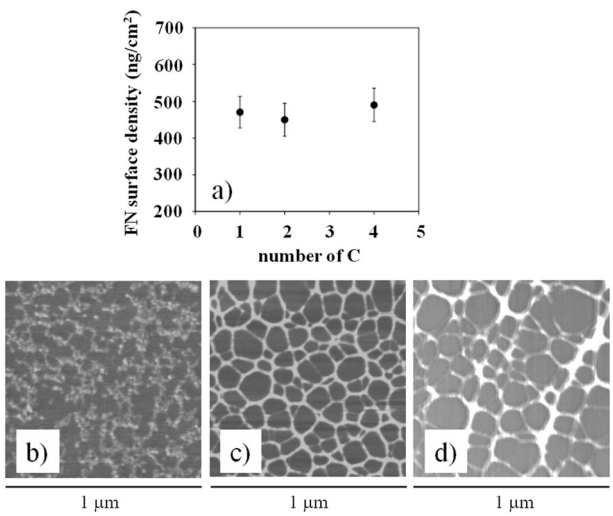

Fig. 2 Fibronectin adsorption and distribution on the material surfaces from a solution of concentration 20 mg mL^{-1}. (a) Fibronectin surface density as a function of the length of the side group (number of C). (b) Fibronectin (white) distribution on the different substrates as observed by the phase magnitude in AFM. PMA (b), PEA (c), and PBA (d).

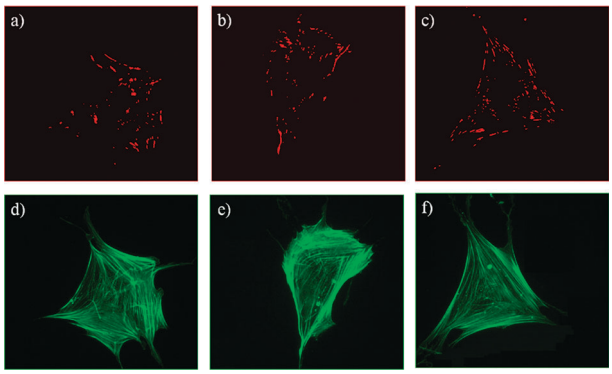

Fig. 3 Focal adhesion formation (vinculin, top) and actin cytoskeleton organization after 3 days on FN coated surfaces for cells on the different surfaces. PMA (a, d), PEA (b, e) and PBA (c, f).

Fig. 2b–d shows the AFM images of the adsorbed FN on the different substrates from a protein solution of concentration 20 μg mL^{-1} for 10 min (concentration used to coat the material surfaces prior to cell culture). The adsorption process gives rise to the formation of FN networks on PEA ($x = 2$) and PBA ($x = 4$) but not on PMA ($x = 1$), on which only dispersed FN molecules are observed. Detailed explanation on the influence of the concentration of the protein solution on FN distribution throughout the material surface on this family of polymers are detailed elsewhere.[31] Overall, Fig. 2 shows that the same density of FN is adsorbed on every substrate but in different conformation that gives rise to altered supramolecular distribution on the material surface: globular aggregates on PMA ($x = 1$) and organized fibrils on PEA and PBA ($x = 2$, $x = 4$).

Cell adhesion

Cell adhesion was evaluated after 3 days of culture on the FN-coated surfaces to ensure a good adhesion on the surface and still be individual cells.[43] In this way we focus on cell–material interaction rather than cell–cell interaction. It is important to note that the initial cell–material interaction occurred in serum-free medium. Thus, initial cell contact is only *via* the initial layer of adsorbed FN on the material surfaces. Fig. 3 demonstrates the overall morphology of cells following staining for actin. Cells were noted to present prominent actin fibers terminating at well-developed focal adhesion complexes, as depicted in Fig. 3 for vinculin.

The area of the focal plaques was quantified by image analysis for several ($n > 10$) cells on the different substrates and focal plaque frequency distribution presented in Fig. 4. The distribution of focal plaques was similar for cells on the three surfaces, with a higher fraction (40%) of the smallest adhesions (<1 μm^2) that decreased monotonically up to 6 μm^2 (Fig. 4b). In contrast, there are significant differences for the distribution of the absolute number of focal contacts per cell: Fig. 4c demonstrates higher numbers of focal contacts of 1, 2 and 3 μm^2 on the substrate with the longest side group ($x = 4$). This is more clearly observed in Fig. 4d illustrating the total number of focal adhesions per cell which was qualitatively higher on $x = 4$.

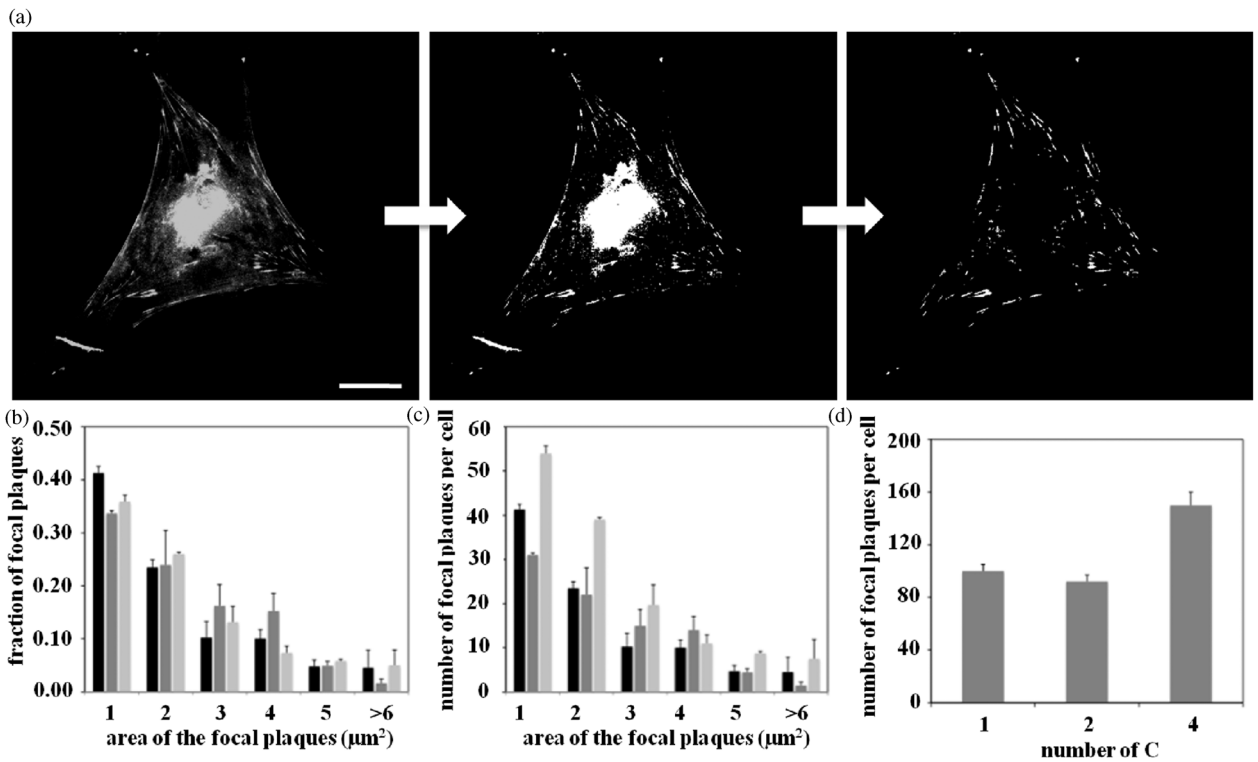

Fig. 4 Image analysis of focal adhesions. (a) The sequential process described in the text to delimitate focal adhesion plaques from the original image is shown for one cell. (b) Size distribution of focal adhesion plaques on the different substrates as quantified by image analysis. (c) Distribution of the number of focal plaques per cell as a function of the area of the focal plaques. (d) Total number of focal plaques per cell on the different substrates (number of C).

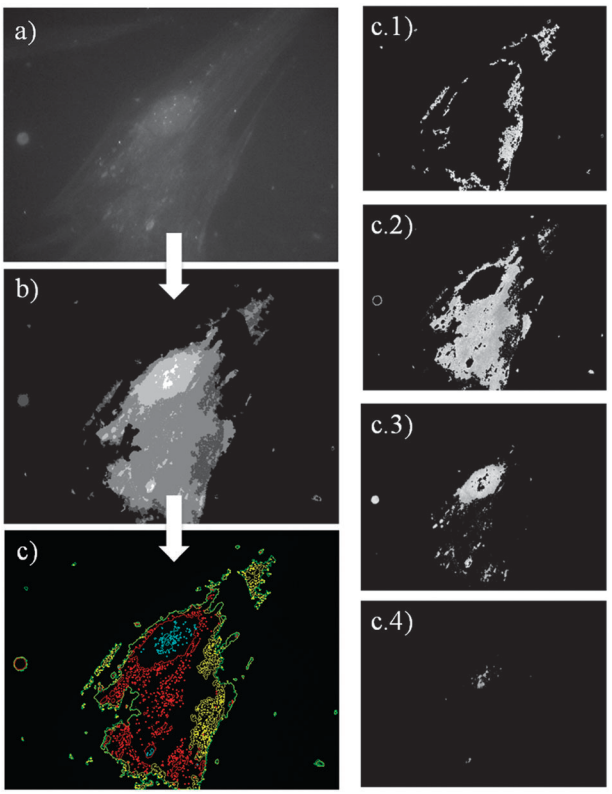

Fig. 5 Image analysis for quantification of osteoblastic markers (osteocalcin, osteopontin and Runx2). The figure shows the sequential process described in the Experimental section.

Cell differentiation

The effect of the subtle variations in surface chemistry on mesenchymal or skeletal stem cell differentiation was examined in basal media. Taking into account the range of stiffness measured on these materials, differentiation along the osteoblastic lineage was determined. The immunofluorescence staining of secreted matrix-associated proteins (OCN and OPN) were used as markers of osteoblastic differentiation.[6–8] We have developed a methodology to quantify immunofluorescence images for osteogenic markers, as detailed in the Experimental section and shown in Fig. 5 for osteocalcin (OCN) secretion on one of the surfaces. Fig. 6 shows representative images for OCN expression on the different substrates examined. Quantification of the images shows non-monotonical dependence for OCN expression as the number of carbons increases in the side group of the substrates. Thus, OCN was upregulated on PMA ($x = 1$) and PBA ($x = 4$), while lower expression was observed on PEA ($x = 2$). The elastic modulus was noted to decrease and surface mobility increases monotonically as the length of the side groups increased (x from 1 to 4). Thus our data show that OCN expression depends non-monotonically on physical properties of the matrix for this family of FN-coated surfaces. Similar results were observed for osteopontin (OPN) secretion on the different substrates (Fig. 7). In contrast, the dependence of the phosphorylation of Runx2 was upregulated for cells on PBA ($x = 4$), although no significant differences were found between PMA ($x = 1$) and PEA ($x = 2$). In all cases, glass was included as a control surface.

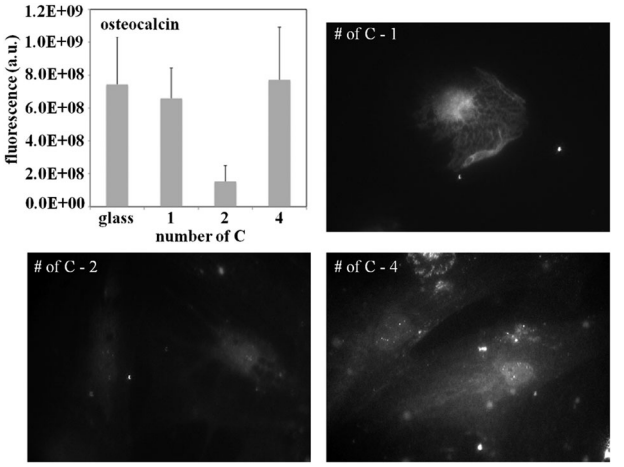

Fig. 6 Osteocalcin staining of osteoprogenitors after 21 days of culture on the different surfaces containing increasing number of carbons in the side group, PMA (1), PEA (2) and PBA (4). The graph shows quantification from images as described previously in the text and Fig. 5.

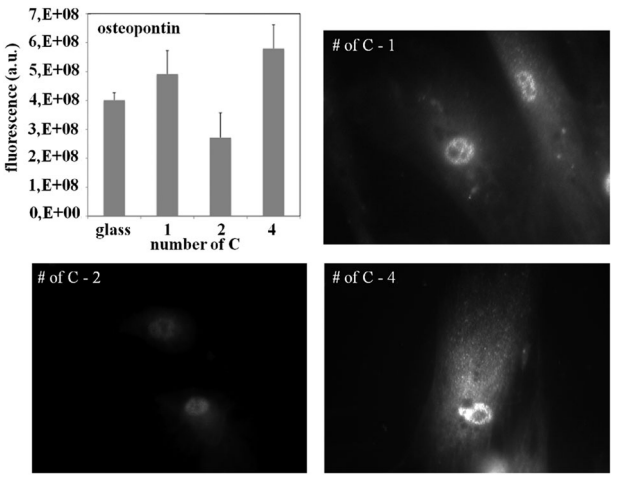

Fig. 7 Osteopontin staining of osteoprogenitors after 21 days of culture on the different surfaces containing increasing number of carbons in the side group, PMA (1), PEA (2) and PBA (4). The graph shows quantification from images as described previously in the text and Fig. 5.

Discussion

Mesenchymal stem cells respond dramatically in both morphology and lineage to physical characteristics of the matrix presented, including surface chemistry,[9] nanotopography[4] and stiffness,[6] even in the absence of soluble factors in the media.[4,6] Here we present evidence of a non-monotonical dependence of mesenchymal stem differentiation on a family of substrates with subtle variations of surface chemistry, namely the sequential addition of methyl groups in the side group of a vinyl chain (Fig. 1). A set of substrates were synthesized with similar surface wettability (Fig. 1b), but monotonically decreasing mechanical properties (the stiffness is accounted for by the elastic modulus in Fig. 1c), and glass transition temperature (Fig. 1d). The glass transition temperature (T_g) is related to the mobility of the polymer chains, which is frozen at temperatures below the glass transition and increases dramatically at temperatures above T_g.[44] More specifically, it has been recently shown that surface layer

mobility is enhanced as the glass transition temperature of the films decreased.[45] It is important to remark here that surface mobility, as accounted by the T_g, is a magnitude whose physical origin is independent of the mechanical moduli of the material: the mobility of the polymer chains is higher, at *e.g.* 37 °C, the lower the T_g of the sample, and while mechanical response involves the deformation of the substrate, surface mobility occurs regardless of the mechanical actions performed on the substrate. That is to say, adsorbed proteins are able to sense surface mobility but remain unaffected by the mechanical properties of the surface.

It is well-known that cell–material interactions occur through the intermediate layer of proteins between the material substrates and the living cells: the amount of adsorbed protein and its conformation direct integrin binding, focal adhesion composition and signalling.[46,47] Approximately the same amount of FN was adsorbed on our family of polymers (Fig. 2a). The measured FN surface density ($\sim$450 ng cm^{-2}) was not dependent on the length of the side group of the polymer chains (x = 1–4). However, the distribution and conformation of the adsorbed FN, which determine its biological activity, showed some variations among the substrates. PEA is a well-studied polymer able to trigger FN organisation upon adsorption, leading to a physiological-like material-driven fibronectin fibrillogenesis in the absence of cells.[48,49] The dynamics of the assembly process for the FN network on PEA has been followed by AFM, and the resulting supramolecular network shown to be biologically active, driving cell adhesion, focal adhesion formation and matrix deposition as well as enhanced myoblast differentiation.[48,49] Similarly, comparable supramolecular organisation of the adsorbed FN layer was found on PEA and PBA after adsorption from a solution of concentration 20 μg mL^{-1} (similar to that used to investigate cell–material interaction) irrespective of the small differences in material chemistry and, consequently, independently of physical properties of these matrices such as either stiffness or surface mobility.[31] By contrast, only globular FN molecules are distributed across the PMA surface (Fig. 2b), which supports the idea that minute variations in polymer chemistry alter FN conformation during adsorption.[30]

Our data show that it is too simplistic to discuss physical properties such as stiffness without considering the absorbed protein layer between the surface and cell. In this study, we show that whilst stiffness changes so does FN conformation. If the activity of the intermediate protein layer at the material interface is neglected, contradictory results are obtained in terms of cell differentiation. For instance, when MC3T3 pre-osteoblastic cells are cultured on polyacrylamide substrates with different mechanical properties—achieved by changing the fraction of the crosslinker—proliferation and osteogenic differentiation were maximized on rigid substrates.[50] In contrast, when the same cell line was cultured on alginate gels of similar mechanical moduli, the cells were found to differentiate faster on the softer substrates.[51] Thus these opposing results, using the same cell line and substrates of similar stiffness, would appear to be a consequence of altered protein activity that occurs due to the chemical modifications of the underlying substrates performed to tailor activity.

FN activity is the same on PEA and PBA, in terms of adsorbed density and supramolecular distribution (Fig. 2), which allowed investigation of the effect of matrix physical properties on cell differentiation, after discarding effects purely related to the organisation of FN at the cell–material interface.[28] The effect of matrix elasticity on mesenchymal stem cell differentiation has been described to occur on synthetic substrates of stiffness that mimic the physiological tissue microenvironment, that for osteoblastic lineages should be in the range of osteoid precursors of bone (25–40 kPa).[4] Fig. 1c shows that the elastic modulus measured for PEA and PBA is one order of magnitude higher (500 kPa) than the stiffness of the natural microenvironment. Thus, since cells must deform the substrate to sense the substrate, taking into account the range of force cells can exert (which range from 1 to 5 nN μm^{-2})[52,53] as well as the distribution of focal adhesions that we have quantified (Fig. 3), it would appear that cells are not able to deform the underlying substrates and, consequently, both PEA (x = 2) and PBA (x = 4) must be sensed as simply rigid substrates by cells. This would indicate that changes are not linked to stiffness.[54]

There is some evidence that the mobility of the adhesion ligands at the cell–material interface improves cell behavior. Increasing the tether length of a synthetic peptide containing the RGD and the synergy sequence PHSRH to the underlying substrate enhanced cell spreading and reduced the time to form focal adhesions.[55] Similarly, disorder can be interpreted as one form of mobility, and it was found that disordered nanopatterns of RGD on a bioinert background provided a much greater variety of ligand density for positive cell adhesion.[56] On a more physical ground, disorder and mobility are related to the same thermodynamic magnitude: entropy; which would suggest that surfaces of higher entropy would favor cell adhesion. Furthermore, osteoblast differentiation of skeletal stem cells has been found to be enhanced on disorder nanoscale topographies,[6] which can be equally described as surfaces of increased entropy as compared to the order system with qualitatively the same nanotopography. In this study we demonstrate that even if FN is adsorbed with the same density and supramolecular distribution on PEA (x = 2) and PBA (x = 4), cell differentiation along the osteoblastic lineages is enhanced on PBA (x = 4) (Fig. 6–8) on which more focal adhesions are found (Fig. 4). The glass transition temperature of PBA (x = 4) is 30 °C below that of PEA (x = 2), which means that surface mobility is enhanced on PBA.

This property can also be related to the fact that the organization of FN takes place with faster dynamics on PEA than PBA, *i.e.* from lower concentrations of the adsorbing FN solution, on PBA than on PEA.[31] Strikingly, surface mobility not only enhanced cell adhesion, as previously shown for other systems,[51] as seen by the higher number of focal adhesion plaques found in PBA (x = 4) than PEA (x = 2) (Fig. 4), but it targets skeletal stem cell differentiation along the osteoblastic lineage with greater efficiency, as shown by the upregulation of characteristic osteoblastic markers osteocalcin, osteopontin and Runx2 (Fig. 6–8). In addition, it has been recently shown that subtle differences in –CH_3 chain lengths (an associated surface mobility) are able to induce changes in MSC phenotype,[57] supporting a direct effect of surface mobility on cell differentiation.

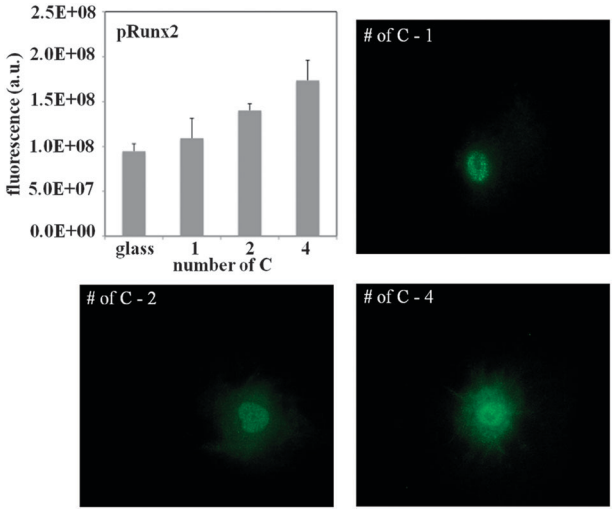

Fig. 8 Phosphorylation of Runx2 staining of osteoprogenitors after 1 day of culture on the different surfaces containing increasing number of carbons in the side group, PMA (1), PEA (2) and PBA (4). The graph shows quantification from images as described previously in the text and Fig. 5.

Conclusions

The system based on a vinyl chain with the side groups $–COO(CH_2)_xH$, and $x = 1, 2, 4$, allows assessment of the influence of minute variations in surface chemistry in protein adsorption and cell differentiation. Thus, transition from $x = 1$ to $x = 2$ drastically alters FN distribution at the cell–material interface, such that other physical parameters of the matrix (*e.g.* stiffness) do not play any role in cell differentiation. However, FN activity (surface density and distribution) is similar on the surfaces $x = 2$ and $x = 4$, which allows the investigation of the role of other physical properties of the matrix in cell differentiation. Stiffness of this family of surfaces is well above the physiological elastic moduli of the osteoid precursors of bone, and consequently they behave simply as stiff surfaces for the cell mechanomachinery. Nevertheless, surface mobility is higher on $x = 4$ than $x = 2$, demonstrated by the glass transition temperature of the system, which enhanced cell adhesion and enhanced differentiation of mesenchymal stem cells to the osteoblastic lineage.

Thus, this study has demonstrated surface mobility, and its quantification by the glass transition temperature, as a new physical parameter of the matrix able to direct skeletal stem cell differentiation. Our findings indicate the potential to modulate stem and progenitor cell commitment along desired lineages through surface mobility of the underlying material surface with implications therein for reparative strategies in, for example, an increasing elderly population.

Acknowledgements

The support of the Spanish Ministry of Science and Innovation through project MAT2009-14440-C02-01 is acknowledged. CIBER-BBN is an initiative funded by the VI National R&D&i Plan 2008–2011, Iniciativa Ingenio 2010, Consolider Program, CIBER Actions and financed by the Instituto de Salud Carlos III with assistance from the European Regional Development Fund. Dalby and Oreffo are supported by BBSRC grant NanoStem (BB/G008868/1).

Notes and references

1 M. F. Pittenger, *Methods Mol. Biol.*, 2008, **449**, 27–44.
2 M. F. Pittenger, A. M. Mackay, S. C. Beck, R. K. Jaiswal, R. Douglas, J. D. Mosca, M. A. Moorman, D. W. Simonetti, S. Craig and D. R. Marshak, *Science*, 1999, **284**, 143–147.
3 R. McBeath, D. M. Pirone, C. M. Nelson, K. Bhadriraju and C. S. Chen, *Dev. Cell*, 2004, **6**, 483–495.
4 A. J. Engler, S. Sen, H. L. Sweeney and D. E. Discher, *Cell (Cambridge, Mass.)*, 2006, **126**, 677–689.
5 N. Huebsch, P. R. Arany, A. S. Mao, D. Shvartsman, O. A. Ali, S. A. Bencherif, J. Rivera-Feliciano and D. J. Mooney, *Nat. Mater.*, 2010, **9**, 518–526.
6 M. J. Dalby, N. Gadegaard, R. Tare, A. Andar, M. O. Riehle, P. Herzyk, C. D. W. Wilkinson and R. O. C. Oreffo, *Nat. Mat.*, 2007, **6**, 997–1003.
7 S. Oh, K. S. Brammer, Y. S. J. Li, D. Teng, A. J. Engler, S. Chien and S. Jin, *Proc. Natl. Acad. Sci. U. S. A.*, 2009, **106**, 2130–2135.
8 L. E. McNamara, R. J. McMurray, M. J. P. Biggs, F. Kantawong, R. O. C. Oreffo and M. J. Dalby, *J. Tissue Eng.*, 2010, **18**, 120623.
9 J. E. Phillips, T. A. Petrie, F. P. Creighton and A. J. García, *Acta Biomater.*, 2010, **6**, 12–20.
10 J. M. Curran, R. Chen and J. A. Hunt, *Biomaterials*, 2006, **27**, 4783–4793.
11 F. Grinnell, *J. Cell Biol.*, 1986, **103**, 2697–2706.
12 U. S. Schwarz and I. B. Bischofs, *Med. Eng. Phys.*, 2005, **27**, 763–772.
13 J. D. Sipe, *Ann. N. Y. Acad. Sci.*, 2002, **961**, 1–9.
14 C. Werner, T. Pompe and K. Salchert, *Adv. Polym. Sci.*, 2006, **203**, 63–93.
15 A. J. Garcia, *Adv. Polym. Sci.*, 2006, **203**, 171–190.
16 K. Anselme, M. Bigerelle, B. Noel, E. Dufresne, D. Judas, A. Iost and P. Hardouin, *J. Biomed. Mater. Res.*, 2000, **49**, 155–166.
17 R. O. Hynes, *Cell (Cambridge, Mass.)*, 2002, **110**, 673–687.
18 A. J. García, *Biomaterials*, 2005, **26**, 7525–7529.
19 D. E. Discher, P. Janmey and Y. L. Wang, *Science*, 2005, **310**, 1139–1143.
20 R. J. Pelham, Jr. and Y. Wang, *Proc. Natl. Acad. Sci. U. S. A.*, 1997, **94**, 13661–13665.
21 L. A. Flanagan, Y. E. Ju, B. Marg, M. Osterfield and P. A. Janmey, *Neuroreport*, 2002, **13**, 2411–2415.
22 A. Schneider, G. Francius, R. Obeid, P. Schwinté, J. Hemmerlé, B. Frisch, P. Schaaf, J. C. Voegel, B. Senger and C. Picart, *Langmuir*, 2006, **22**, 1193–1200.
23 P. L. Ryan, R. A. Foty, J. Kohn and M. S. Steinberg, *Proc. Natl. Acad. Sci. U. S. A.*, 2001, **98**, 4323–4327.
24 J. Y. Wong, A. Velasco, P. Rajagopalan and Q. Pham, *Langmuir*, 2003, **19**, 1908–1913.
25 C. M. Lo, H. B. Wang, M. Dembo and Y. L. Wang, *Biophys. J.*, 2000, **79**, 144–152.
26 I. B. Bischofs and U. S. Schwarz, *Proc. Natl. Acad. Sci. U. S. A.*, 2003, **100**, 9274–9279.
27 K. Saha, A. J. Keung, E. F. Irwin, Y. Li, L. Little, D. V. Schaffer and K. E. Healy, *Biophys. J.*, 2008, **95**, 4426–4438.
28 A. S. Rowlands, P. A. George and J. J. Cooper-White, *Am. J. Physiol.: Cell Physiol.*, 2008, **295**, C1037–C1044.
29 J. S. Park, J. S. Chu, A. D. Tsou, R. Diop, Z. Tang, A. Wang and S. Li, *Biomaterials*, 2011, **32**, 3921–3930.
30 Y. H. Bae, P. A. Johnson, C. A. Florek, J. Kohn and P. V. Moghe, *Acta Biomater.*, 2006, **2**, 473–482.
31 N. Brizuela-Guerra, C. González-García, V. Llopis, J. C. Rodríguez Hernández, D. Moratal, P. Rico and M. Salmerón-Sánchez, *Soft Matter*, 2010, **6**, 4748–4755.
32 P. Rico, J. C. Rodríguez Hernández, D. Moratal, M. Monleón Pradas, G. Altankov and M. Salmerón-Sánchez, *Tissue Eng., Part A*, 2009, **15**, 3271–3281.
33 N. A. Otsu, *IEEE Trans. Syst. Man Cybern.*, 1979, **9**, 62–66.
34 X. B. Yang, H. I. Roach, N. M. Clarke, S. M. Howdle, R. Quirk, K. M. Shakesheff and R. O. C. Oreffo, *Bone (Amsterdam, Neth.)*, 2001, **29**, 523–531.

35 D. Howard, K. Partridge, X. Yang, N. M. P. Clarke, Y. Okubo, K. Bessho, S. M. Howdle, K. M. Shakesheff and R. O. C. Oreffo, *Biochem. Biophys. Res. Commun*., 2002, **299**, 208–215.
36 P. J. Simmons and B. Torok-Storb, *Blood*, 1991, **78**, 55–62.
37 J. T. Triffitt, C. J. Joyner, R. O. Oreffo and A. S. Virdi, *Biochem. Soc. Trans*., 1998, **26**, 21–27.
38 X. Yang, R. S. Tare, K. A. Partridge, H. I. Roach, N. M. Clarke, S. M. Howdle, K. M. Shakesheff and R. O. Oreffo, *J. Bone Miner. Res*., 2003, **18**, 47–57.
39 S. H. Mirmalek-Sani, R. S. Tare, S. M. Morgan, H. I. Roach, D. I. Wilson, N. A. Hanley and R. O. Oreffo, *Stem Cells*, 2006, **24**, 1042–1053.
40 R. C. Gonzalez, R. E. Woods and S. L. Eddins, *Digital Image Processing using MATLAB*, Prentice-Hall, Upper Saddle River, NJ, 2003.
41 R. C. Gonzalez and R. E. Woods, *Digital Image Processing*, Prentice-Hall, Upper Saddle River, NJ, 2007.
42 *MATLAB Image Processing Toolbox User's Guide,* The MathWorks, Inc., Natick, MA, 2006.
43 L. E. McNamara, T. Sjöström, K. E. V. Burgess, J. J. W. Kim, E. Liu, S. Gordonov, P. V. Moghe, R. M. D. Meek, R. O. C. Oreffo, B. Su and M. J. Dalby, *Biomaterials*, 2011, **32**, 7403–7410.
44 G. E. Strobl, *The physics of polymers: concepts for understanding their structures and behavior*, Springer, Berlin, 1997.
45 Z. Yang, Y. Fujii, F. K. Lee, C. H. Lam and O. K. C. Tsui, *Science*, 2010, **328**, 1676–1679.
46 B. G. Keselowsky, D. M. Collard and A. J. García, *Biomaterials*, 2004, **25**, 5947–5954.
47 B. G. Keselowsky, D. M. Collard and A. J. García, *J. Biomed. Mater. Res., Part A*, 2003, **66**, 247–259.
48 D. Gugutkov, C. González-García, J. C. Rodríguez Hernández, G. Altankov and M. Salmerón-Sánchez, *Langmuir*, 2009, **25**, 10893–10900.
49 M. Salmerón-Sánchez, P. Rico, D. Moratal, T. Lee, J. E. Schwarzbauer and A. J. García, *Biomaterials*, 2011, **32**, 2099–2105.
50 C. B. Khatiwala, S. R. Peyton and A. J. Putnam, *Am. J. Physiol.: Cell Physiol*., 2006, **290**, C1640–C1650.
51 H. J. Kong, T. H. Polte, E. Alsberg and D. J. Mooney, *Proc. Natl. Acad. Sci. U. S. A*., 2005, **102**, 4300–4305.
52 N. Q. Balaban, U. S. Schwarz, D. Riveline, P. Goichberg, G. Tzur, I. Sabanay, D. Mahalu, S. Safran, A. Bershadsky, L. Addadi and B. Geiger, *Nat. Cell Biol*., 2001, **3**, 466–472.
53 C. G. Galbraith, K. M. Yamada and M. P. Sheetz, *J. Cell Biol*., 2002, **25**, 695–705.
54 G. C. Reilly and A. J. Engler, *J. Biomech*., 2010, **43**, 55–62.
55 W. Kuhlman, I. Taniguchi, L. G. Griffith and A. M. Mayes, *Biomacromolecules*, 2007, **8**, 3206–3213.
56 J. Huang, S. V. Grater, F. Corbellini, S. Rinck, E. Bock, R. Kemkemer, H. Kessler, J. Ding and J. P. Spatz, *Nano Lett*., 2009, **9**, 1111–1116.
57 J. M. Curran, F. Pu, R. Chen and J. A. Hunt, *Biomaterials*, 2011, **32**, 4753–4760.